JAST, Vol. 13, No. 1, pp.67-76

JAST
Journal of Aerospace Science and Technology

Science Article

GROWTH AND COLLAPSE OF A CAVITATION BUBBLE INSIDE A RIGID CYLINDER: EFFECT OF MEMBRANE TENSION

Amireh Norbaskhsh[1]
1- Department of Mechanical Engineering, Bu-Ali Sina University, Hamedan,
Bu-Ali Sina University, Shahid Mostafa Ahmadi Roshan Street, Hamedan
Email: ***nourbakhsh@basu.ac.ir**

In this paper, growth and collapse of a cavitation bubble inside a rigid cylinder with a compliant coating (a model of human's vessels) are studied using Boundary Integral Equation and Finite Difference Methods. The fluid flow is treated as a potential flow and Boundary Integral Equation Method is used to solve Laplace's equation for velocity potential. The compliant coating is modeled as a membrane with a spring foundation. At the interface between the fluid and the membrane, the pressure and normal velocity in the flow are matched to the pressure and normal velocity of the membrane using linearized condition. The effects of the parameters describing the flow (the fluid density, the initial cavity size and its position) and the parameter describing the compliant coating (membrane tension) on the interaction between the fluid and the cylindrical compliant coating are shown throughout the numerical results. It is shown that the bubble life time slightly decreases by increasing membrane tension.

Keywords: *bubble, collapse, membrane tension, Boundary element method.*

Introduction

Cavitation bubbles are produced in a liquid flow when the static pressure is below the saturated vapor pressure. These bubbles move with liquid flow and violently collapse in high pressure regions. Violent collapse of the bubbles is believed to be one of the most important parameters in mechanical damage of hydraulic machineries and structures. They have also beneficial effects in medicine and Lithotripsy surgery. Experimental and numerical results show that during the collapse phase of a cavitation bubble near a rigid boundary a liquid jet is developed on the side of bubble far from the rigid boundary and directed towards the boundary. This liquid jet threads the collapsing bubble, creating a toroidal bubble. Cavitation bubbles behavior near various boundaries depends on material, dimension and shape of the surface and the bubble distance from the nearby boundary. Dynamics of a vapour bubble generated due to a local energy input in the vicinity of different kinds of surfaces is of significant importance in medicine

1 . Assistance Professor

Received Date: 12 Nov. 2020
Accepted Date: 12 Dec. 2020

and industry. Numerical and experimental results have shown that a vapour bubble generated due to a local energy input in the vicinity of a rigid boundary is attracted by the rigid surface. In this case during the collapse phase of the bubble, a liquid micro jet is developed on the far side of the bubble from the rigid boundary and is directed towards it [1-3]. Numerical results have also shown that during the growth and collapse of a vapour bubble generated due to a local energy input beneath a free surface, the vapour bubble has a different behaviour. In this case, the vapour bubble is repelled by the free surface. During the collapse phase a liquid micro jet is developed on the closest side of the bubble to the free surface and is directed away from it [4-6]. In the case of the pulsation of the vapour bubble near a rigid surface, the impingement of the liquid micro jet to the rigid surface is an important cause of mechanical erosion. Experimental investigations also show that at the end of the collapse phase of the vapour bubble and just before its rebound a shock wave is emitted in the liquid domain. The emission of the shock wave inside the liquid domain is also cause of rigid surface destruction [7].

The laboratory investigations of Rheingans [8] and Lichtman et al. [9] have indicated that surfaces coated with elastomeric materials are more resistant to cavitation erosion. Theorizing that this increased resistance to erosion might result from a redirection of the re-entrant jet in a manner similar to a free surface. Gibson and Blake [10] photographed the collapse of a spark-generated cavitation bubbles in the vicinity of walls covered by elastomeric coating of several compositions. They found that under some circumstances the collapse was modified such that a jet was indeed directed away from the wall. A more detailed set of experiments with spark-generated bubble adjacent to a compliant surface has been reported by shima et al. [11] and Tomita and Shima [12]. The position and size of the cavity and the thickness of the compliant surfaces were varied. The results showed again that it is possible to redirect the re-entrant jet away from the wall with a properly designed compliant coating and gave detailed information on the history of the cavity shape. No measurements of the motion of the compliant surface were reported. In the numerical investigation of Duncan and Zhang [13], the compliant coating was modeled as a membrane with a spring foundation. At the interface between the fluid and membrane, the pressure and normal velocity in the flow are matched to the pressure and normal velocity of the membrane using linearized condition.

The use of shock waves to destroy kidney stones is practiced in hospitals throughout the world. Although over two million successful lithotripsy treatments have occurred, there is still much to be learned about the physical mechanisms of stone destruction, its possible side effects, and how the technique can be improved. Scientists are studying the technique for better understanding of the mechanisms involved (Wolfrum [14]). The investigations focus on the Spark Discharge Method, in which a shock wave is produced by the explosion associated with an underwater spark discharge. The spark discharge occurs in an ellipsoidal reflector located outside the patient's body. The reflector concentrates up to 90% of the energy released from the discharge into a shock wave focused on the internal kidney stone. Stones and tissue are destroyed through the action of tensile stresses within and at the surface of the stone, and through cavitation, which produce surface-damaging microjets. When a liquid is placed under tensile stress it can rip apart, producing a bubble or cavity. When pressure surrounding a bubble falls below the vapor pressure of the liquid, the bubble fills with vapor and grows explosively. The bubble collapses violently when pressure returns. If the collapse occurs near a boundary, such as the targeted kidney stone, a high velocity liquid jet is formed that impacts the boundary with a great force. These extremely violent processes are thought to play a major role in stone destruction and associated tissue damage (Shervani-Tabar et al. [15, 16]).

A nanoboat armed with a cavitation toolkit may be the future basis for the first practical and versatile nanoassembler. Cavitation reentrant jets could even be used to propel the nanoboat. The potential of cavitation as the next wave in nanomanufacturing is examined in the light of current technology (Leclair et al. [17], Patek and Caldwell [18]).

In the present paper, the growth and collapse of a cavity near a compliant wall is explored numerically. In particular, the above-mentioned potential flow model for the fluid motion has been coupled to a rigid cylinder with a compliant coating modeled as a spring-backed membrane. This coating is characterized by its mass per unit area , membrane tension , spring stiffness per unit area and maximum radius of the bubble ( ) (m) (T) (K R_m). The coating is coupled to the flow model through the normal velocity and the pressure at the flow-coating interface, linearized boundary conditions are applied at the location of the undisturbed membrane surface. A detailed account of the theory behind this fully interactive model and its numerical implementation are described in

section 2. Results and discussions are presented in section 3 which show the effects of the coating and cavity characteristics on the growth and collapse phases of the bubble. The numerical results are in good agreement with the experimental results of Gibson and Blake [10] and Shima et al. [11] about dynamics of vapor bubble near a flat compliant coating. The conclusions of the work are given in section 5.

Numerical implementation

A schematic representation of the vapor cavity, the cylinder and the coordinate system used in the calculations is given in Figure 1.

In the numerical model, the surface of the bubble is divided into M part by planes which are perpendicular to the Z-coordinate. For overcoming the problem of non-smoothing linear surface elements, The Cubic Spline Surface elements are used to approximate the surface of the bubble (see Figure 2). The interface between the fluid and the wall is modeled by a set of MN elements consisting of Ncs elements on the membrane with equal length and (MN- Ncs) elements on the rigid wall with non-equal length. Field points (nodes) are taken at the middle of each element. If S_j is the j^{th} element then for a point P_i on the bubble surface, approximating form of equation is shown in the discretized form of:

$$2\pi\phi(p_i)+\sum_{J=1}^{M}\left\{\phi(q_J)\int_{S_J}\frac{\partial}{\partial n}\left[\frac{1}{|p_i-q_j|}\right]dS\right\} = \sum_{J=1}^{M}\left\{\frac{\partial}{\partial n}[\phi(q_J)]\int_{S_J}\left[\frac{1}{|p_i-q_j|}\right]dS\right\} \quad (1)$$

If $\psi=\frac{\partial \emptyset}{\partial n}$ then the above equation is expressed as a system of linear equations:

$$2\pi\phi(p_i)+\sum_{j=1}^{M}H_{ij}\phi(q_j)=\sum_{j=1}^{M}G_{ij}\psi(q_j) \quad (2)$$

Where H_{ij} and G_{ij} are integral terms in equation (1).

By knowing velocity potential $\emptyset$ on the surface of the bubble, normal velocity on the surface of the bubble, ψ is obtained from equation (2).

The calculation is started when the bubble is in its minimum initial volume. ϵ and P_0 must be selected in so suitable manner that the bubble grows to a maximum volume with a non-dimensional radius equal to 1. Variable non-dimensional time step for a bubble that contains a mixture of constant pressure vapor and ideal gas is obtained from:

$$\Delta t=\min\left(\frac{\Delta\phi}{\frac{P_\infty-P_v}{P_\infty-P_c}+\frac{1}{2}\left|\nabla\phi_i\right|^2+\delta^2(Z_i-\gamma)}\right) \quad (3)$$

Where $\Delta\phi$ is a constant quantity that controls the maximum velocity potential increase at each time step.

By using equation (2), ψ is obtained. Tangential velocity on the surface is obtained from the known distribution of velocity potential ϕ along the bubble surface. By having the normal and tangential velocities, radial and vertical velocities on the bubble surface are obtained. Since the variations of the normal velocity on the surface of the bubble at the end of the collapse phase and at the early stages of the bubble rebound are very high, then the Rounge-Kutta method of the second order is employed for numerical simulation of the bubble evolution during its pulsations. $i\ r$ and $i\ Z$ are position coordinate of $i\ p$ and $i\ \phi$ is velocity potential at time t . Position of point $i\ p$ and velocity potential $i\ \phi$ at time $t+\Delta t$ are obtained from:

$$r_{i1}=r_i(t)+u_{i1}\Delta t$$
$$Z_{i1}=Z_i(t)+v_{i1}\Delta t$$
$$\phi_{i1}=\phi_i(t)+\left[\frac{\partial\phi}{\partial t}\right]_{i1}\Delta t$$
$$r_i(t+\Delta t)=r_i(t)+\frac{1}{2}(u_{i1}+u_{i2})\Delta t+O(\Delta t^2) \quad (4)$$
$$Z_i(t+\Delta t)=Z_i(t)+\frac{1}{2}(v_{i1}+v_{i2})\Delta t+O(\Delta t^2) \quad (5)$$
$$\phi_i(t+\Delta t)=\phi_i(t)+1/2\left(\left[\frac{\partial\phi}{\partial t}\right]_{i1}+\left[\frac{\partial\phi}{\partial t}\right]_{i2}\right)\Delta t+O(\Delta t^2) \quad (6)$$

Where u_{i1} and u_{i2} are intermediate radial velocities and also v_{i1} and v_{i2} are intermediate vertical velocities. Intermediate quantity of the velocity potential derivative with respect to time is given as:

$\left[\frac{\partial\phi}{\partial t}\right]_{i1}$ and $\left[\frac{\partial\phi}{\partial t}\right]_{i2}$.

By having velocity potential on the bubble surface at time $t+\Delta t$ and by knowing this fact that the fluid velocity perpendicular to the rigid surface is zero, the normal velocity of the membrane must found to solve the system of M+MN equations at time $t+\Delta t$.

The application of Runge-Kutta method to the membrane equations yields:

$$\eta_{i1} = \eta_i(t) + \eta_{i1}\Delta t \tag{7}$$

$$\xi_{i1} = \xi_i(t) + [\frac{\partial \xi}{\partial t}]_{i1}\Delta t \tag{8}$$

$$\eta_i(t+\Delta t) = \eta_i(t) + \tfrac{1}{2}(\xi_{i1} + \xi_{i2})\Delta t + O(\Delta t^2) \tag{9}$$

$$\xi_i(t+\Delta t) = \xi_i(t) + 1/2\left(\left[\frac{\partial \xi}{\partial t}\right]_{i1} + \left[\frac{\partial \xi}{\partial t}\right]_{i2}\right)\Delta t + O(\Delta t^2)$$

(10)

Discretization of the membrane equation gives:

$$\left[\frac{\partial \xi}{\partial t}\right]_{j+1}^{i} = \frac{T}{m}\left[\frac{\eta_{j+1}^{i} - 2\eta_j^i + \eta_{j-1}^i}{(\Delta Z)^2}\right] - \frac{K}{m}\eta_j^i + (P_w(Z_j, t_i) - P_\infty)/m \tag{11}$$

In Eq. (11),$\partial\eta/\partial$Z is zero at $\mathrm{Z} = 0$ and η is zero at $\mathrm{Z} \pm \mathrm{R}_{cs}$. The former boundary condition is a consequence of symmetry, while the latter boundary condition is a consequence of the attachment of the membrane to the rigid boundary at $\mathrm{Z} \pm \mathrm{R}_m$. The reflected waves that are introduced by this attachment are caused by physical processes rather than numerical inaccuracies.

The numerical forms of the boundary conditions at the flow-membrane interference, are:

$$[\frac{\partial \eta}{\partial t}]_j^i = \xi_j^i = [-\frac{\partial \varphi}{\partial r}]_j^i \tag{12}$$

$$P_j^{i+1} - P_\infty = -\rho\frac{\varphi_j^{i+1} - \varphi_j^i}{t_{i+1} - t_i} \tag{13}$$

Initially the velocity on the membrane is equal to zero and the solution of the problem is similar to the case of the rigid surface. The calculations at time Δt have turned out to be difficult. In proceeding to time Δt to obtain the required value of ϕ on the membrane, the position of the nodes on the cavity and the corresponding values of ϕ are obtained from equation (6). In order to get ϕ on the membrane surface, the value of $\partial\phi / \partial n$ on the membrane must be known for solving equation (2). However computing $\partial\phi / \partial n$ requires the pressure on the membrane at $t = 0$.

Unfortunately, this pressure is the quantity that was being sought in the first place. An iterative scheme was devised to overcome this problem [13]. On the first iteration, the pressure on $r = R$ at $t = 0$ is computed assuming the coating to be rigid. This allows for the computing of an approximate value of $\partial\phi / \partial n$ on the membrane at $t = \Delta t$. The calculation then proceeds for a few time steps with a relatively stiff compliant boundary. The pressure on the wall soon settles down to a distribution that is nearly constant in time. At this point, the calculation is restarted with the equilibrated pressure distribution and a softer wall. This procedure is repeated until the desired coating properties are achieved.

Results and Discussions

In this solid-fluid interaction problem, there are a number of independent variables. For the fluid, these variables include the maximum radius of the cavity, R_m , ratio of the cylinder diameter to the maximum radius of the bubble, λ , the pressure difference, $P_{inf} - P_c$ and the density of the fluid,ρ. For the coating, the variables are the mass per unit area, m , the tension,T , the spring constant, K , and the width of the coating, R_m. The dimensionless forms of these variables are given as:

$$r = r/R_m \tag{14}$$

$$Z = Z/R_m \tag{15}$$

$$\lambda = DIAM/R_m \tag{16}$$

$$t = \frac{t}{R_m}\left(\frac{P_{\inf} - P_C}{\rho}\right)^{1/2} \tag{17}$$

$$\Phi = \frac{\phi}{R_m}\left(\frac{\rho}{P_{\inf} - P_C}\right)^{1/2} \tag{18}$$

$$\Psi = \psi\left(\frac{\rho}{P_{\inf} - P_C}\right) \tag{19}$$

$$M^* = \frac{m}{\rho R_m} \tag{20}$$

$$T^* = \frac{T}{R_m \Delta P} \tag{21}$$

$$K^* = \frac{KR_m}{\Delta P} \tag{22}$$

Where is R the radius of the cavity, P_{inf} is pressure in the far field and DIAM is diameter of the cylinder. Also ϕ is the velocity potential and ψ is normal velocity on the bubble boundary and on the membrane surface and is time t.

In performing the calculations, two modes of instability were found. The first occurs if the tension is too large and can be stabilized by reducing the time step. For instance, with $T^* \geq 0.75$ the stability of calculation is

impossible. This instability appeared as an oscillation in the membrane surface with high spatial frequency that starts near $Z = \pm R_{cs}$ and spreads inward. It is suspected that this instability is related to the instabilities generally found in the solution to hyperbolic equations like the one describing the coating. The second instability that is one which is considered in this research occurs when the mass of the membrane is too low or the membrane radius is too large. In this research it was not possible to obtain a stable calculation with M^* low enough to make the collapse spherical. This instability occurs in the start of calculations and thus the pressure distribution on the surface of the compliant coating and adjacent rigid boundary has not been converged to a stable pressure distribution.

The general behavior of the cavity and coating Units

The cavity profiles, wall pressure profiles and wall velocity profiles at various times during the growth and collapse of a cavity in four different cylinders are presented first to give the reader an overview of the phenomenon. The profiles of the cavity at various times for the four cases are presented in Figure 3. In all cases, λ is equal to 3. Figure 3a depicts the growth and the collapse of the cavity in a rigid cylinder, while in Figures 3b, 3c and 3d the wall has a compliant section with the properties of $R_{cs} = 2.5\ R_m$ and $T^* = 0.0025$. In each of these cases M^* and K^* are equal and their values are 3.5, 2.0 and 1.5 in Figures 3b, 3c and 3d, respectively. The cavity shapes shown here are typical of all the calculations presented in this paper. When the coating becomes softer, the volume of the bubble at the end of the collapse phase becomes smaller.
With inspection of the bubble life time, it is observed that when the coating becomes softer, the bubble life time decreases. Dimensionless bubble life time near a rigid surface is 4.43174 and in Figure 3b reduces to 4.26421 and by softer membranes in Figure 3c and 3d the bubble life time reduces to 4.23232 and 4.20825 respectively. The distribution of the pressure on the cylinder wall during the growth and collapse phases of the bubble corresponding to Figure 3a-3d are shown in Figures 4a- 4d, respectively. The time of each pressure distribution is corresponding to the time of each profile in Figure 3. In each distribution, the pressure has a maximum at $z = 0$ and tends to zero as z tends to infinity. In the compliant wall cases, there are wiggles in the pressure distributions near the boundary. It is observed from profiles that for the four cases when the membrane becomes softer, the minimum pressure decreases very slightly. Since the pressure on the wall during the growth phase is less than P_{inf}, the membrane moves towards the cavity and during the collapse phase, the membrane moves away from the cavity.
The normal velocity profiles on the wall are presented in Figure 5. The normal velocity on the rigid part of the boundary is, of course, zero. The velocity profiles in the all other three cases are similar and only one of them is shown. At the early stages of the growth phase, the distributions are all negative and at the early stages of the collapse phase are positive. A maximum value of the normal velocity can be seen at $z = 0$ and near the outer edge of the compliant wall the velocity decreases to zero rapidly. It is obvious that the velocities generally increase with the softness of the coating (for smaller M^* and K^*).

The effect of T^*

In the previous results, the small value of the membrane tension, $T^* = 0.0025$ has rendered its influence negligible. In order to explore the influence of the membrane tension, a set of calculations were performed with M^*=1.5, $\lambda = 3$ $R_{cs} = 2.5R_m$, $R_m = 0.00002m$, $K^* = 2.0$ and three values of T^*: 0.025, 0.25 and 0.75 The profiles of the cavity versus time are very similar and therefore are not shown here. The life time of cavity at various T^* is shown in Figure 6. It is obvious that the life time of the cavity slightly decreases by increasing T^*
The distributions of the pressure on the cylinder wall during the growth and collapse phases of the bubble are shown in Figure 7a-7c. In performing the calculations, a mode of instability is found when the tension is too large and can be stabilized by reducing the time step. In the case of $T^* \geq 0.75$ the stability of calculation is impossible. This instability appeared as an oscillation in the membrane surface with high spatial frequency that starts near $z = \pm R_{cs}$ and spreads inward. It is suspected that this instability is related to the instabilities generally found in the solution to hyperbolic equations like the one describing the coating. In each distribution, the pressure has a maximum at Z=0 and tends to P_{inf} as Z=0 tends to be $\pm\infty$

The distributions of vertical velocity on the wall of cylinder at the end of the growth and collapse phases are shown in Figure 8a-8b for three values of T^* At the early stages of the growth phase, the distributions are all negative and at the early stages of the collapse phase are positive. The most prominent effect of the tension is in the region near the outer edge of the compliant surfaces. When the tension is very small, the velocity of the membrane is nearly constant near the edge of membrane and suddenly drops to zero at $Z = \pm R_{cs}$ When the tension is larger, the region of negative velocity near the edge of the coating develops at the late stages of the collapse phase. This is consistent with the higher resistance to membrane curvature in the calculations with higher tension. At $T^* = 0.75$ the instability is seen in velocity profiles that are discussed beforehand. The other properties of the coating and the cavity are not shown here because they are similar for all three values of T^* .

An extensive set of experimental data on the behavior of the cavities near a compliant wall is reported by Shima et al. [11]. Unfortunately, there are several principal differences between the conditions of the present research and the conditions of the experimental work of Shima et al. [11]. Probably the most important difference is that in the experimental work of Shima et al. the wall is flat, while in the present paper, the wall is cylindrical. Another difference between the experimental work of Shima et al. and the present research concerns the construction of the coating. The coating used by shima et al. was consisted of an untensioned layer of rubber backed by a layer of foam. The rubber layer had finite thickness and so a finite bending stiffness, while in the numerical model there was no bending stiffness.

Concluding Remarks

A numerical method for simulation of the collapse of a cavity bubble inside a rigid cylinder with a compliant coating has been presented. In the numerical model, the surface of the bubble is divided into M part by planes which are perpendicular to Z-coordinate. For overcoming the problem of non-smoothing linear surface elements, The Cubic Spline Surface elements are used to approximate the surface of bubble. The interface between the fluid and the wall is modeled by a set of MN elements consisting of N_{cs} elements on the membrane with equal length and $(MN - N_{cs})$ elements on the rigid wall with non-equal length. Field points (nodes) are taken at the middle of each element. In this solid-fluid interaction problem, there have been a number of independent variables. For the fluid, these variables have included the maximum radius of the cavity,R_m , the ratio of the cylinder diameter to the maximum radius ratio, λ , the pressure difference, $P_{inf} - P$ and the density of the fluid, ρ. For the coating, the variables have been the mass per unit area,m , the tension, T, the spring constant,K , and the width of the coating, R_{cs}. In different manners, the effects of these parameters have been inspected. When the wall is compliant, it is possible to create a spherical collapse for a fairly range of wall parameters. The value of $T^* = \frac{T}{R_m \Delta P}$ (where is the tension) does not dominate the physics of the interaction when it is small. The distributions of vertical velocity on the wall of cylinder at the end of the growth and collapse phases were found for different values of T^*. At the early stages of the growth phase, the distributions are all negative and at the early stages of the collapse phase are positive.

With inspection of bubble life time, it is observed that when the coating becomes softer, the bubble life time decreases, the minimum pressure decreases very slightly, the normal velocities on the wall generally increase and the transposition of the center of the compliant coating increases.

In performing the calculations, two modes of instability were found. The first occurs if the tension is too large and can be stabilized by reducing the time step. For instance, with $T^* = 0.75$ the stability of calculation is impossible. This instability appeared as an oscillation in the membrane surface with high spatial frequency that starts near $z = \pm R_{cs}$ and spreads inward. It is suspected that this instability is related to the instabilities generally found in the solution to hyperbolic equations like the one describing the coating. The second instability that is one which is considered in this research occurs when the mass of the membrane is too low or the membrane radius is too large.

References

1. Blake, J. R., Taib, B. B., and Doherty, G. Transient cavities near boundaries; Part 1. Rigid boundary. J. Fluid Mech, Vol. 170 (1986), 479.
2. Blake, J. R., Gibson, D. C. Cavitation bubbles near boundaries. Ann. Rev. Fluid Mech, Vol. 19 (1987) 99- 123.
3. Soh, W. K., Shervani-Tabar, M. T. Computer model for a pulsating bubble near a rigid surface. Computational Fluid Dynamics Journal. Vol. 3, 1 (1994) 223-236.
4. Blake, J. R., Taib, B. B., and Doherty, G. Transient cavities near boundaries; Part 2. Free surface. J. Fluid Mech, Vol. 181 (1986) 197-212.
5. Blake, J. R., Gibson, D. C. Growth and collapse of a vapour cavity bubble near a free surface. J. Fluid Mech, Vol. 111 (1981) 123-140.
6. Shervani-Tbar, M. T. Computer study of a cavity bubble near a rigid boundary, a free surface, and a compliant wall. PhD Thesis, University of Wollongong, Wollongong, Australia (1995).
7. Lauterborn, W. Cavitation and coherent optics. Cavitation and Inhomogenities in Underwater Acoustics, Proceedings of the First International
Conference, , Fed. Rep. of Germany, Lauterborn (Ed.), Springer-Verlag, (1980) 3-12.
8. Rheingans, W. J. Resistance of various materials to cavitation damage. Report of 1956 Cavitation symposium, published by Am. Soc. Mechanical. Engrs (1956).
9. Lichtman, J. Z., Kallas, D. H., Chatten, C. K, and Cochran, E. P. Study of corrosion and cavitation erosion damage. Transactions, Am. Soc. Mechanical. Engrs (1958).
10. Gibson, D. C., and Blake, J. R. The growth and Collapse of Cavitation Bubble near Deformable Surfaces. appl. sci. res, Vol. 38 (1982) 215-224.
11. Shima, A., Tomita, Y., Gibson, D. C., and Blake, J. R. The growth and collapse of cavitation bubbles near composite surface. J. Fluid Mech, Vol. 203 (1989) 199- 214.
12. Tomita, Y., and Shima, A. Destructive action of cavitation bubbles collapsing near boundaries. Shock focussing effect in medical science and sonoluminescence (2003) 73- 109.
13. Duncan, J. H., and Zhang, S. On the interaction of a collapsing cavity and a compliant wall. J. Fluid Mech, Vol. 226 (1991) 401-423.
14. Wolfrum, B. Cavitation and shock wave effects on biological systems. PhD Thesis, Department of Physic, University of Gottingen (2004).
15. Shervani-Tabar, M. T., Rezaee-Barmi, A., and Mahmoudi, S. M. Velocity field and pressure distribution around two parts of a cavitation bubble after its Splitting near a rigid boundary. Fifth international Symposium on cavitation (Cav 2003), November 1-4, Osaka, Japan. Cav03-GS-2-008.
16. Shervani-Tabar, M. T., Rezaee-Barmi, A., and Mahmoudi, S. M. Velocity field and pressure distribution around a collapsing cavitation near a rigid boundary during the Necking phenomenon. Fifth international Symposium on cavitation (Cav 2003), November 1-4, Osaka, Japan. Cav03-GS-2-007.
17. LeClair ML, Barros EF, Guvench MG. Cavitation and the Future of Nanotechnology. Ninth Foresight Conference on molecular nanotechnology (2005).
18. Patek, S. N., and Caldwell, R. L. Extreme impact and cavitation forces of a biological hammer: Strike forces of the peacock mantis shrimp Odontodactylus scyllarus. Journal of Experimental Biology, Vol. 208 (2005) 3655- 3664.
19. Rayleigh, L. On the pressure developed in a liquid during collapse of a spherical void. Phil. Mag, Vol. 34 (1917) 94-98.
20. Best, J. P. The Dynamics of Underwater Explosions. PhD Thesis, Department of Mathematics, University of Wollongong (1991) 1-48.

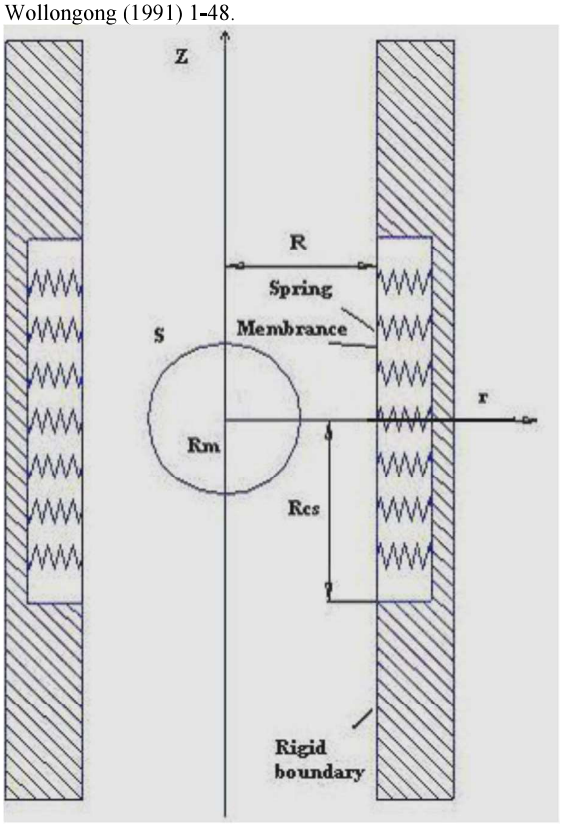

Fig. 1: Schematic representation of the coordinate system and the initial position of the cavity and the compliant boundary.

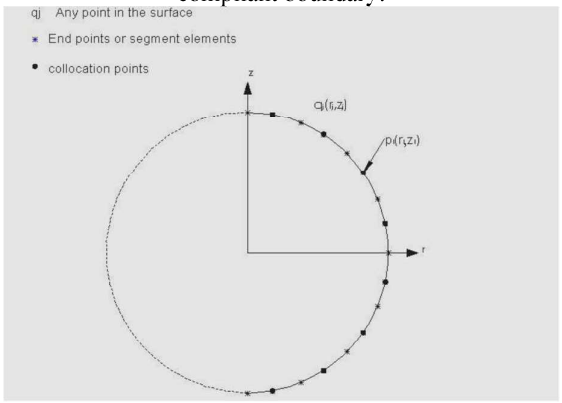

Fig 2: The Cubic Spline elements on the surface of the bubble

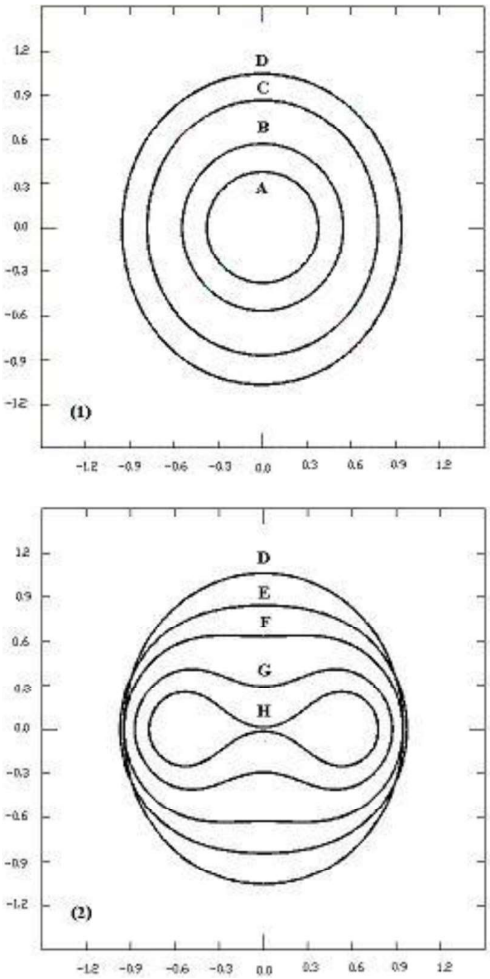

Fig 3a: (1) growth phase: A. t=0.00364 B. 0.289 C. 0.86492 D. 2.39814
(2) collapse phase: D. t=2.39814 E. 2.89929 F. 3.64984 G. 4.11513
H. 4.43174.

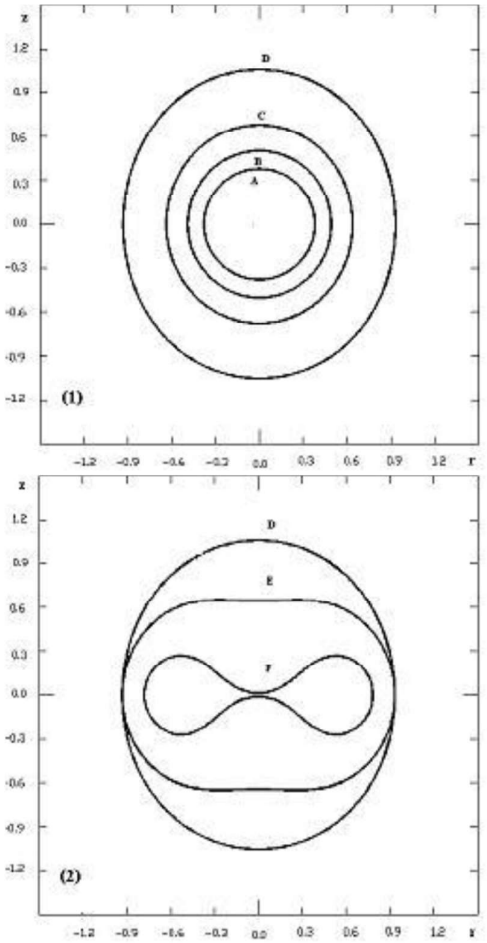

Fig 3b: (1) growth phase: A. t=0.00364 B. 0.44621 C. 0.89757 D. 2.29865
(2) collapse phase: D. t=2.29865 E. 2.56579 F. 4.26421.

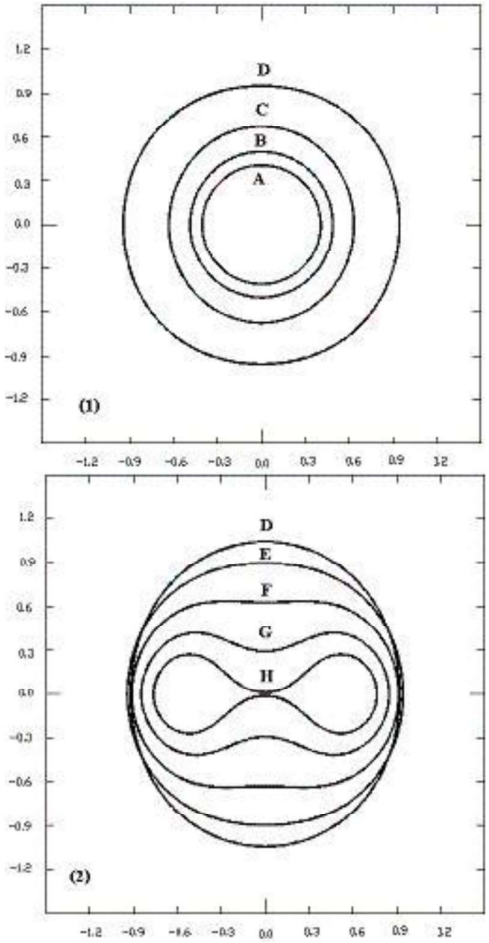

Fig 3c: (1) growth phase: A. t=0.00364 B. 0.45478 C. 0.91106 D. 2.27526
(2) collapse phase: D. t=2.27526 E. 2.89429 F. 3.47035 G. 3.92036 H. 4.23232.

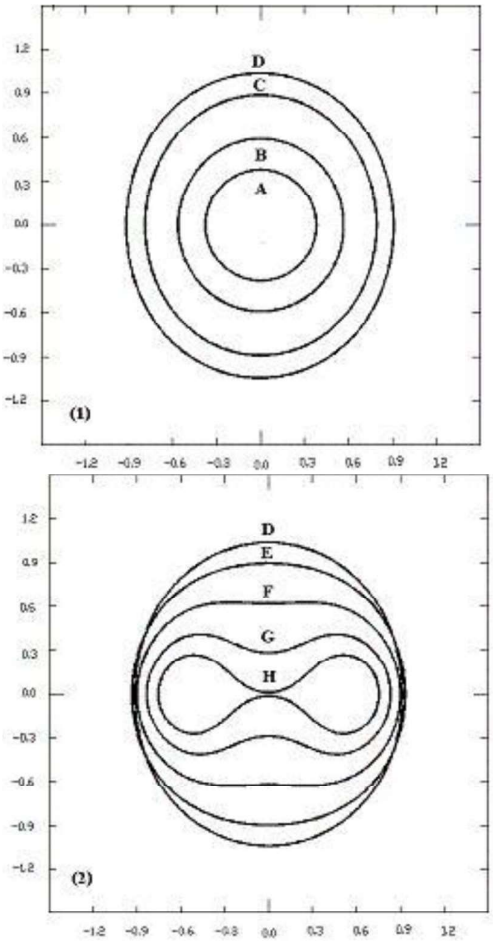

Fig 3d: (1) growth phase: A. t=0.00364 B. 0.30914 C. 0.92105 D. 2.24921
(2) collapse phase: D. 2.24921 E. 2.958 F. 3.4647 G. 3.90482 H. 4.20825.

$T^* = 0.0025$. $R_{cz} = 2.5R_m$, $R_m = 0.00002m$; (c) $M^* = 2.0$. $K^* = 2.0$. $T^* = 0.0025$. $R_{cz} = 2.5R_m$, $R_m = 0.00002m$;(d) $M^* = 1.5$. $K^* = 1.5$. $T^* = 0.0025$. $R_{cz} = 2.5R_m$, $R_m = 0.00002m$.

Fig 3: Cavity profiles at various times for four cases with λ=3: (a) Rigid surface;

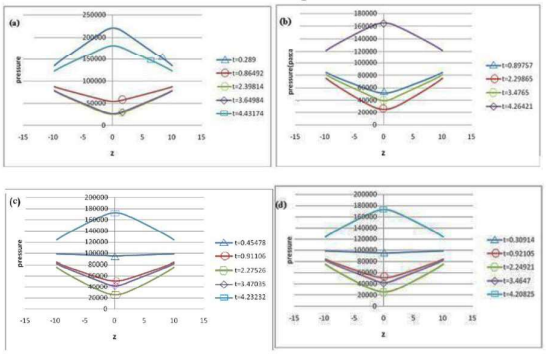

Fig 4: Pressure profiles on the cylinder wall at times and conditions corresponding to figure 3.

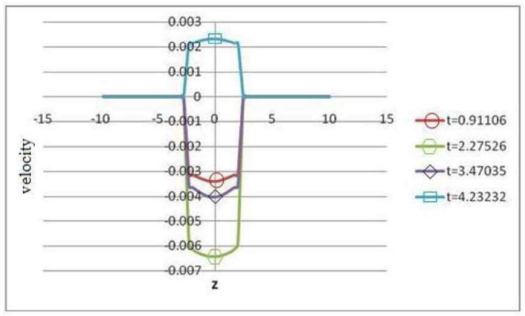

Fig 5: Normal velocity profiles on the wall at various times for the case with λ=3 $M^* = 3.5$,$K^* = 3.5$,$T^*0.0025$, $R_{cs} = 2.5\ R_m$, R_m=0.00002m